Hindawi
International Journal of Polymer Science
Volume 2023, Article ID 2842385, 16 pages
https://doi.org/10.1155/2023/2842385

Research Article

Optimization of the Synthesis Parameters and Application of Cellulose Nanocrystals as Binders in Capacitors

Carlos F. Castro-Guerrero,[1] **Andrea González-Benítez**,[2] **Abisaí Rodríguez-Rodríguez**,[2] **Filemón Delgado-Arroyo**,[2] **Ulises León-Silva**,[3] **Ana B. Morales-Cepeda**,[4] **Francisco A. López-González**,[2] **Arturo Rodas-Grapain**,[2] **and Mario R. Díaz-Guillén**[2]

[1]*CONAHCyT-Tecnológico Nacional de México, Campus Ciudad Madero, Parque Industrial Tecnia, Bahía de Aldair S/N, Altamira 89603, Mexico*
[2]*Gerencia de Materiales y Procesos Químicos, Instituto Nacional de Electricidad y Energías Limpias, Reforma 113, Col. Palmira, Cuernavaca, C. P. 62490 Morelos, Mexico*
[3]*Centro de Investigación en Ingeniería y Ciencias Aplicadas de la Universidad Autónoma del Estado de Morelos, Av. Universidad 1001, Col. Chamilpa, Cuernavaca, C. P. 62209 Morelos, Mexico*
[4]*Tecnológico Nacional de México, Campus Ciudad Madero, Parque Industrial Tecnia, Bahía de Aldair S/N, Altamira 89603, Mexico*

Correspondence should be addressed to Carlos F. Castro-Guerrero; cfcastrog80@gmail.com

Received 27 February 2023; Revised 21 June 2023; Accepted 22 June 2023; Published 7 July 2023

Academic Editor: Qinglin Wu

Cellulose nanocrystals (CNCs) are a very versatile material, and optimizing the reaction conditions to obtain them is vital for cost savings, purity, selectivity, or performance. In this study, the reaction conditions of the CNCs were tested, as well as their application as binders for the fabrication of electrodes of a symmetric capacitor (based on activated carbon). The resulting CNCs were physicochemically characterized using Fourier transform infrared spectroscopy, thermogravimetric analysis, X-ray diffraction, atomic force microscopy, and its capacitive properties using cyclic voltammetry (CV). It was found that the best reaction conditions were at 45°C, 30 and 45 minutes, and 64 wt%. The CNCs were used as a binder, as they conferred stability to the electrodes and prevented the crumbling of the activated carbon electrodes. The CV measurements showed a capacitor behavior; CNCs can be used in energy storage applications.

1. Introduction

Cellulose nanocrystals (CNCs) have attracted a great deal of attention due to their many properties. Recently, Sharma et al. [1] reviewed the applications and processing of CNCs. They found that CNCs have many applications, ranging from the traditional applications of inks or reinforcement of materials to newer applications, such as drug delivery, ion exchange membranes, coatings, self-healing materials, and conductive films. Other recent applications of CNCs are drug delivery matrices, films for food packaging, skin grafting, and parts for wind turbines. [2] In addition, CNCs have the property of being renewable, biodegradable, and non-toxic. CNCs have been produced from cellulosic residues in wastewater [3]. Cellulose was collected from residues in wastewater and isolated, and CNCs were obtained from the recovered cellulose, they showed the characteristic rod-like shape of CNCs. The length of the CNCs was 111–134 nm, with a diameter of 10–14 nm; they were used for improving the mechanical properties of alginate composites, and the alginate modulus was increased in the 42–83% range. The properties of CNCs have made them an attractive material for applications in engineering and many fields. CNCs is a highly crystalline material, and it has the property of forming liquid crystals suspensions after achieving a given concentration, this mesophase is retained upon drying the

material [4]. Tayeb et al. [5] described the applications of nanocellulose in energy applications, among them, capacitors. They focused on cellulose nanofibers (CNFs). CNFs can be used as binding agents in capacitors, giving cohesion to electrodes made of several materials, among them graphite or activated carbon. Commonly used binders are not soluble in water, so pollution by solvents is a great concern [5, 6]. Nanocellulose has also the advantage of lower resistance to electricity than poly(vinyl alcohol).

Nanocellulose has been successfully used to improve the dielectric properties of dielectric paper, which may allow an increment in the lifetime of power transformers. Recently have been synthesized improved flexible composites with CNCs [7], this material has the potential of being used as a flexible CNC paper, as it reduced the brittleness of CNC films. Kraft paper, done with cellulose, is used in the electrical industry as one of the isolating components inside power transformers [8]. Le Bras et al. [9] studied the electrical properties of CNCs and determined that this material conserves the dielectric property of cellulose. Pakharenko et al. [10] fabricated flexible nanocellulose films for applications as substrates of electronic devices. CNFs were obtained, and films of CNFs were made; flexible films were obtained that showed no cracks after 100 times folding, they were subjected to controlled aging to simulate 10 years of aging, and no significant damage was observed on the samples after the aging tests [10].

CNCs can be dispersed in water, but some applications require using them on non-polar compounds. One of these applications is using them on power transformers. Substitutions on the surface of nanocellulose must be performed to make them compatible with non-polar compounds. Several processes and reactions can be used to make substitution reactions [4, 11]. CNCs can be stabilized by charges on the surface, or by steric hindrance of groups at the surface of CNCs [2]. CNC super hydrophobic composites are a promising material for industrial applications [11]; several CNCs composites have been reported in the literature with hydrophobic behavior, making them compatible with non-polar solvents [11]. Recently, Chen et al. [12] fabricated CNFs that were functionalized by esterification, and the resulting nanocomposite was used as the matrix for the controlled delivery of ibuprofen. The groups at the surface of cellulose are susceptible to substitution reactions, making them useful for many purposes.

In this study, we showed the results of the CNC acid-mediated synthesis after varying the synthesis conditions. We describe the effect of variating the reaction conditions on the surface content of sulfate groups on the surface of CNCs. The main objective of this study is to optimize the synthesis parameters of CNCs, to functionalize the surface of CNCs with sulfate groups, and to find the optimal conditions for the subsequent use of CNCs in the technology of improving mineral dielectric oil of power transformers and in capacitors. Results with novel parameters of sulfuric acid concentration, temperature, and small crystallite size are presented, some of them have not been reported in the literature. We also present results showing small crystallite size, with values smaller than reports found in the literature. The resulting CNCs were used as binders in activated-carbon electrodes, these electrodes were tested for supercapacitors. To the best of our knowledge, CNCs have not been used yet as binders. Currently, the research groups use CNFs as binders, not CNCs; this study is the first to use CNCs as binders. The physicochemical characterization obtained by conventional techniques, such as X-ray diffraction (XRD), thermogravimetric analysis (TGA), and Fourier transform infrared spectroscopy (FTIR), is also shown.

2. Methodology

2.1. Purification of Cellulose. Filter paper (Tequimec, Mexico) was used as raw material. The filter paper was purified before CNC isolation by a purification process. The filter paper was boiled in an aqueous solution of sodium hydroxide (NaOH) 0.5 N for 3 hours; then, the filter paper was collected, and the process was repeated. After treatment with NaOH, the filter paper was washed with distilled water until the effluent remained at neutral pH. Then, the filter paper was treated with commercial sodium hypochlorite (NaOCl) for 2 hours at 40°C; after the process, the filter paper was thoroughly washed with distilled water. Then, the filter paper was treated with hydrochloric acid (HCl) 0.01 N for 20 hours at room temperature; after this process, the filter paper was washed with distilled water until the effluent reached a neutral pH. The purified cellulose was dried in a forced convection oven, and then it was ground in a Wiley mill using a 40 mesh sieve.

2.2. Synthesis of CNCs. The purified cellulose was used for the synthesis of CNCs. One gram of cellulose was dispersed in 17.5 mL of a sulfuric acid solution, and vigorously stirred for a given time at a given temperature, these two variables were changed to measure its influence on the CNC properties.

After the hydrolysis, the reaction was quenched by diluting 10-fold with chilled distilled water, and then it was left to settle for 2 hours, the CNCs were decanted, and the process was repeated. Then, the CNCs were dialyzed using distilled water as a buffer solution until the effluent achieved a constant pH. Then, the CNCs were sonicated using a Sonics Vibra-Cell VCX 750, operating at 70% output until a colloidal suspension was formed. The dispersed CNC was filtered using Whatman glass microfiber filters to remove any impurities on the suspension and those introduced during sonication. Finally, the CNC suspensions were stored in a chemical fridge.

We experimented with three variables. The experiment was arranged in a 2^k experimental design. To reduce the number of experiments ($2^3 = 8$), a half-fraction factorial design with two reactions was selected. The experimental design is shown in Table 1.

2.3. Characterization. The CNC suspension was physicochemically characterized; 25 mL of suspension was collected and dried in a convection oven, forming CNC films. The films were characterized with FTIR, using a Bruker spectrophotometer model Equinox 55 equipped with an attenuated

Table 1: Experimental design.

Sample	Hydrolysis time (minutes)	Variable of synthesis Sulfuric acid (H_2SO_4) concentration (wt%)	Temperature (°C)
A1	30 (low)	30 (low)	80 (high)
A2	60 (high)	64 (high)	80 (high)
A3	30 (low)	64 (high)	45 (low)
A4	60 (high)	30 (low)	45 (low)
A5	30 (low)	30 (low)	80 (high)
A6	60 (high)	64 (high)	80 (high)
A7	60 (high)	30 (low)	45 (low)
A8	30 (low)	64 (high)	45 (low)

total reflection (ATR) accessory; the analysis was carried out in the range of 4000–400 cm^{-1} with a resolution of 2 cm^{-1}, and with an average of 64 scans. The CNC films were characterized employing TGA, using a TGA analyzer TA Instruments model TGA 2050; this analysis was performed with a heating rate of 10°C/minutes until 900°C using a nitrogen atmosphere. XRD was done to the samples using an STOE XRD diffractometer model STADI Bragg–Brentano, with a DECTRIS detector model MYTHEN-1K and a cobalt source ($\lambda = 0.1795$ nm); the XRD analysis was done in the range of 4°–85° of 2θ. Crystallinity index was calculated using the Segal method [13]. The method uses the following formula, equation (1)

$$\mathrm{CrI} = \frac{I_{23} - I_{\mathrm{am}}}{I_{23}} \times 100, \quad (1)$$

where CrI is the crystallinity index, I_{23} is the intensity of the peak at 23°, and I_{am} is the Intensity of the amorphous parts at 18°.

Atomic force microscopy (AFM) was made on the samples using a Nanosurf AFM, model Naio, working in contact mode. The samples were deposited on mica substrates. The substrate was cleaved, and immediately it was treated with a drop of poly L-lysine for 5 minutes; then, it was rinsed with distilled water and left to dry in a powder-free environment [13, 14]. Then, the CNC suspension was sonicated, and a drop was deposited on the substrate, followed by another drop. The mica substrate with the CNC suspension was let to dry over filter paper inside a closed, powder-free environment [14].

2.4. Supercapacitors with CNCs. The CNC suspension was used as a binder in supercapacitors. The electrodes were fabricated with activated carbon (Reasol, purified powder) doped with graphite (AC/C); the quantity of graphite was 10 wt%. Activated carbon was measured, and graphite was added; the mixture was stirred vigorously with a spatula for 5 minutes to form a homogenous mixture. 500 g of AC/C mixture was taken, and the CNCs were added dropwise with a Pasteur pipette until a paste was formed. The added amount was 10–15 drops of a 0.16 wt% suspension. The mixture was compressed with a press and dried at 40°C for 24 hours until a solid tablet was formed. The tablets were placed inside copper collectors, having an area of 1 cm^2. As a dielectric membrane, filter paper (Whatman) was used, and placed between the electrodes, and 0.1 mL of NaOH 1.0 N was added to it as an electrolyte. The assembled symmetrical capacitor was placed inside a polycarbonate cell, which was tightly closed with a screwdriver, to prevent the presence of air. Figure 1 shows the scheme of the assembled symmetrical capacitor. The capacitor terminals were connected to the potentiostat and characterized using cyclic voltammetry (CV). All the CV measurements of the capacitor were performed at room temperature (≈24°C) with a two-electrode cell using a Gill 4AC potentiostat/galvanostat; the rate range of 20–100 mV s^{-1} with a potential range −1.8 to 1.8 V.

The estimation of the specific capacitance from the CV was carried out using equation (2) [15]:

$$C_{\mathrm{CV}} = \left[\frac{1}{2 \times \nu \times \Delta V \times m} \int_{V1}^{V2} I(V)\mathrm{d}V\right], \quad (2)$$

where C_{CV} is the specific capacitance in F g^{-1}, ν is the scan rate in V/seconds, m is the mass of the active material in g, ΔV is the potential window in V, and dV represents the area under the CV curve (Q).

Electrochemical impedance spectroscopy (EIS) measurements were carried out using an AC potential amplitude of 10 mV, a frequency interval of 0.5–20 kHz with 100 readings per decade. The EIS measurements were performed at room temperature and controlled by a Gill AC potentiostat/galvanostat. The EIS data were further analyzed using the ZView software.

The EIS data were fitted by a standard equivalent circuit, Figure 2, using the ZView software.

This circuit consists of the R_{ct} (charge transfer resistance) in parallel with a constant phase element (CPE) and these components in series with the R_{s} (electrolyte resistance). The CPE is used instead of a pure capacitor (C_{dl}, double layer capacitance) to take into consideration, the heterogeneities at the metallic surface (roughness, impurities, pores, and cracks). This CPE allows to get a more accurate fit of the EIS data set and its impedance is given by equation (3) [16]:

$$Z_{\mathrm{CPE}} = A^{-1}(i\omega)^{-n}, \quad (3)$$

where A is the proportionality coefficient, ω is the angular frequency, and i is the imaginary number. n is an exponent related to the phase shift and can be used as a measure of surface irregularity.

3. Results and Discussion

3.1. Fourier Transform Infrared Spectroscopy. The FTIR spectra are shown in Figure 3. The samples that were synthesized with a low acid concentration (30 wt%, corresponding to A4 and A5) have a low intensity compared with the other samples. A weak intensity of the bands suggests that they have a high content of amorphous cellulose, because, theoretically,

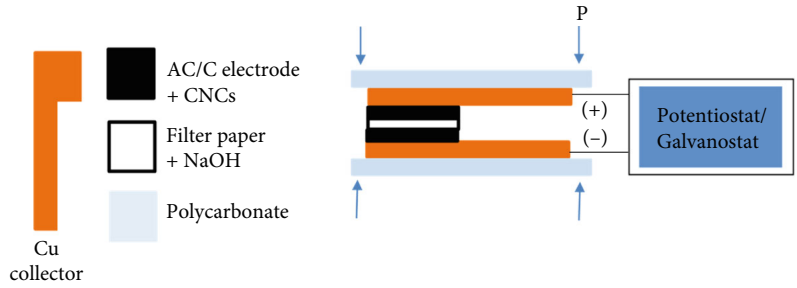

Figure 1: Scheme of the symmetric capacitor.

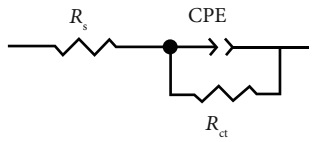

Figure 2: Standard equivalent circuit model.

the intensity and definition of those bands are associated with the crystallinity of cellulosic samples [17, 18]. Samples A1 and A3 show spectra corresponding to the polymorph I of cellulose, their bands suggest a crystalline sample. The samples had no band in the 1800–1600 cm^{-1} region; this region corresponds to carbonyl groups, and its absence suggests that the nanocrystals were not in the oxidized form (i.e., no carboxyl groups are present), but in the sulfated form. It also indicates that the purification process removed lignin and hemicelluloses.

The band at the 3300 cm^{-1} region is associated with the OH groups present in the CNCs. The OH band has two peaks, this shape is present at the same region in spectra of CNCs [13], as opposed to the OH band with one peak typically seen in organic compounds and untreated cellulose.

There are peaks located at 1159 and 894 cm^{-1}, corresponding to the glycosidic C–O–C bond (see Figure 3). This bond links the anhydroglucose units, which in turn form the cellobiose units that are the monomers of cellulose. The rest of the bands observed in the spectra are bending and stretching vibrations characteristic of C–O, C–H, and C–H_2, which are present on the nanocellulose molecule.

The small band located at 815 cm^{-1} corresponds to the C–O–S vibration, this is attributed to the presence of sulfate groups $(SO_4)^{2-}$ introduced during the acid hydrolysis [3], this band can be seen in Figure 4. The change in the band in the samples can be observed in Figure 4. Sample A2 has a very weak intensity, suggesting a low sulfate content, samples A4 and A5 have a low intensity. Samples A1 and A3 have a stronger intensity than the aforementioned samples, suggesting a higher sulfate content.

3.2. Thermogravimetric Analysis. Figure 5(a) shows the thermograms of the CNCs samples. It can be seen in the figure that the samples A2, A4, and A6 have a thermal degradation behavior similar to that of pure cellulose [19], with a thermal degradation onset at 230°C–250°C; then, followed by a rapid degradation with an inflection point at 350°C. There is a weight loss observed between 300°C and 400°C, this loss accounts for 75 wt% of the specimen, and above 800°C the gradual decomposition continues until achieving a weight loss of 85–95 wt%. The thermal degradation is slower after 400°C, whereas the degradation behavior of pure cellulose is more homogeneous. Of these samples, two A2 and A6 were done with high values of time and temperature, suggesting that the harsher reaction conditions caused carbonization of samples as suggested by the brownish colour of the suspension; it has been reported that synthesis at 65°C, a lower temperature than the value used in this study causes dehydration [20, 21]. The other sample, A4 was synthesized with a low sulfuric acid concentration.

On the other hand, samples A1, A3, A7, and A8 show a slower and more complex thermal degradation, a typical degradation behavior of CNCs. This observation correlates with the FTIR spectra of samples A1 and A3, confirming the higher sulfate content of those samples. Figure 5(a) shows that for this group of samples, there is a first step of degradation in the 130°C–150°C range, where the weight loss is about 40 wt%; then there is a second step between 200°C and 300°C, which is slow and gradual. Other steps with a moderate slope are seen in Figure 5(a) until the weight loss is around 80 and 85 wt% above 800°C. The samples A3 and A8, which were synthesized under the same conditions have shoulders at 325°C and 560°C. In literature, several reports are stating that CNCs have a more complex thermal degradation behavior [22–26], and that the sulfate groups are very labile having an effect that the thermal degradation temperature of CNCs is below 300°C, and above that temperature the slope of the degradation curve is gentler compared with the curve of degradation behavior of pure cellulose. The reports in the literature also mention that the thermal degradation of CNCs spans a wider range than that of pure cellulose. Sulfuric acid hydrolysis also causes many free ends of chains in CNCs [23], further catalyzing the degradation of CNCs. Some reports also state that CNC samples have many inflection points as those observed in samples A1, A3, A7, and A8 [22]. Jordan et al. [21] reported a low sulfate content when CNCs were synthesized for 30 minutes, 62 wt% of H_2SO_4, and 50°C, the reported sulfate content found by conductometric titration was 134 mmol kg^{-1}, this sample is similar to the conditions of A3 and A8; however, the sulfuric acid concentration and temperature are different to our report. In the same study of Jordan et al., when the conditions were 60 minutes, 65 wt%, and 55°C, the sulfate content

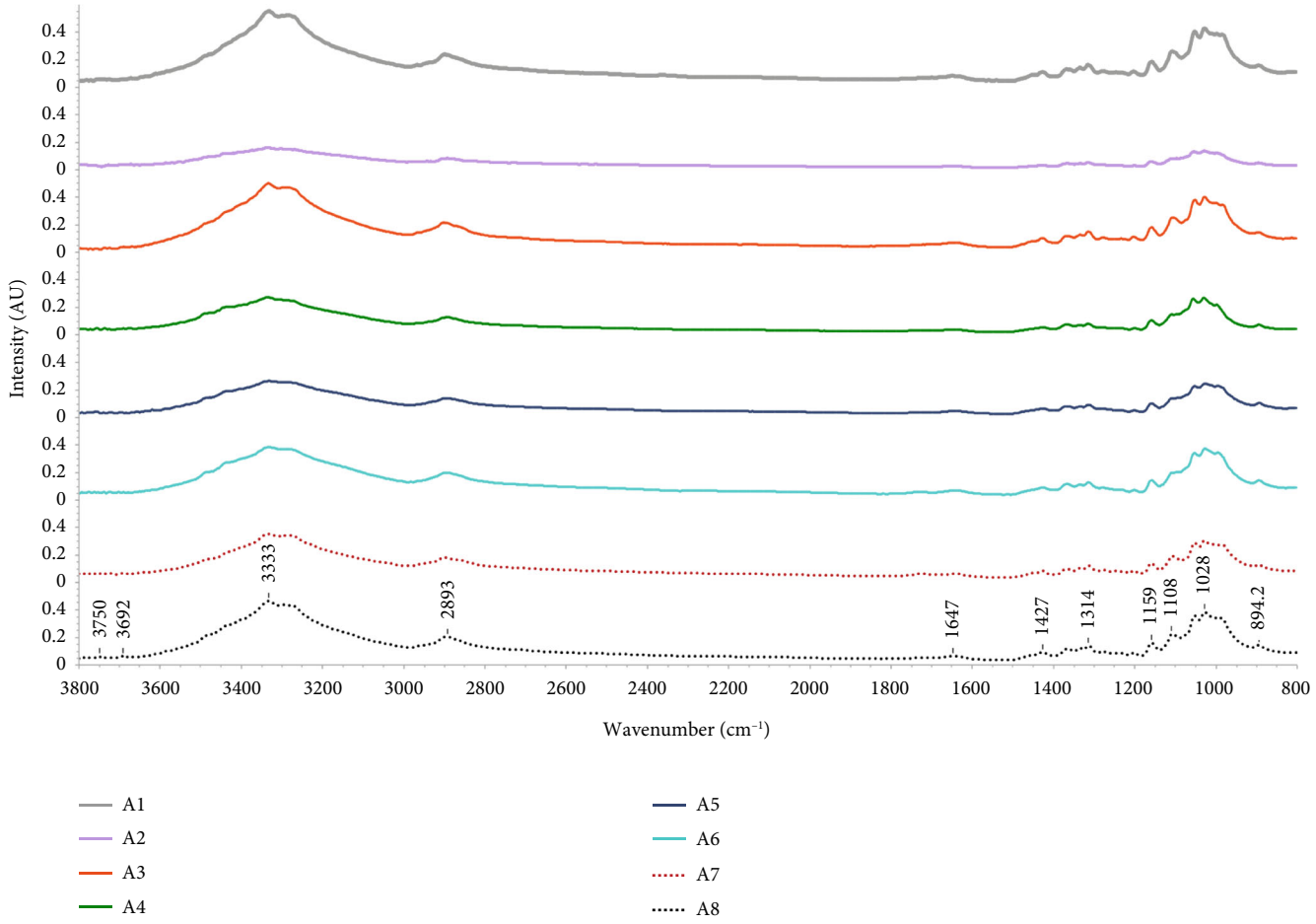

Figure 3: FTIR spectra of CNC samples.

was 197 mmol kg^{-1}; this is similar to the reaction conditions of A2 and A6, but in our study, the temperature is 80°C. The highest sulfate content was found by Jordan et al., when the conditions were 90 minutes, 65 wt% of H_2SO_4, and 60°C, with a sulfate content of 308 mmol kg^{-1} [21].

The comparison between the aforementioned samples suggests that samples A2, A4, and A6 have a lower content of sulfate groups as compared with samples A1, A3, A7, and A8. This observation is consistent with the results observed in the FTIR section for samples A2 and A4. The samples A2 and A6 were synthesized with 60 minutes of reaction time and 80°C of temperature, which leads to carbonization and a lower degree of oxidation in comparison with the samples synthesized with the same reaction time (A3 and A8), but with the standard value of H_2SO_4 content, 64% and 45°C of temperature. In this last case (A3 and A8), the reaction time and temperature are lower, but the sulfuric acid concentration is the same, 64 wt%; however, the reaction conditions are milder and there is no carbonization, and thus the reaction introduces more sulfate groups on the surface of CNCs than in the samples synthesized with harsher conditions, the result is that the thermograms show a different behavior suggesting that the samples had a higher content of sulfate groups.

The samples A2, A4, and A6 were done with the same concentration of time, 60 minutes. The temperature was varied using the values of 45°C (A4) and 80°C (A2 and A6). The sulfuric acid concentration was varied too using the values of 30 wt% (A4) and 64 wt% (A2 and A6). The thermograms suggest that the degradation behavior is more similar to that of cellulose compared with the degradation behavior of nanocellulose.

Samples A3 and A8 were done with the same reaction conditions: time 30 minutes, 64 wt% of H_2SO_4, and 45°C. The degradation behavior of the samples is similar to that of nanocellulose. The behavior of the TGA's curves is almost the same, this suggests that the samples are repeatable. The TGA and FTIR results suggest that the optimal conditions are 64 wt% of H_2SO_4 and 45°C, this result of optimal conditions is in line with previous works in literature [20], and the thermal behavior suggests that the samples have sulfate groups on the surface, unlike in the case of samples A2, A4, and A6. The sulfate groups contribute to stabilizing the CNCs suspensions due to the surface charge that they have, they avoid aggregation of CNCs. Samples A1 and A7 show similar behavior too. In the case of sample A7, the reaction conditions are the same as A4, indicating that they are not repeatable. The sample A1 was synthesized with the conditions of 30 minutes, 30 wt% of H_2SO_4, and 80°C, the higher

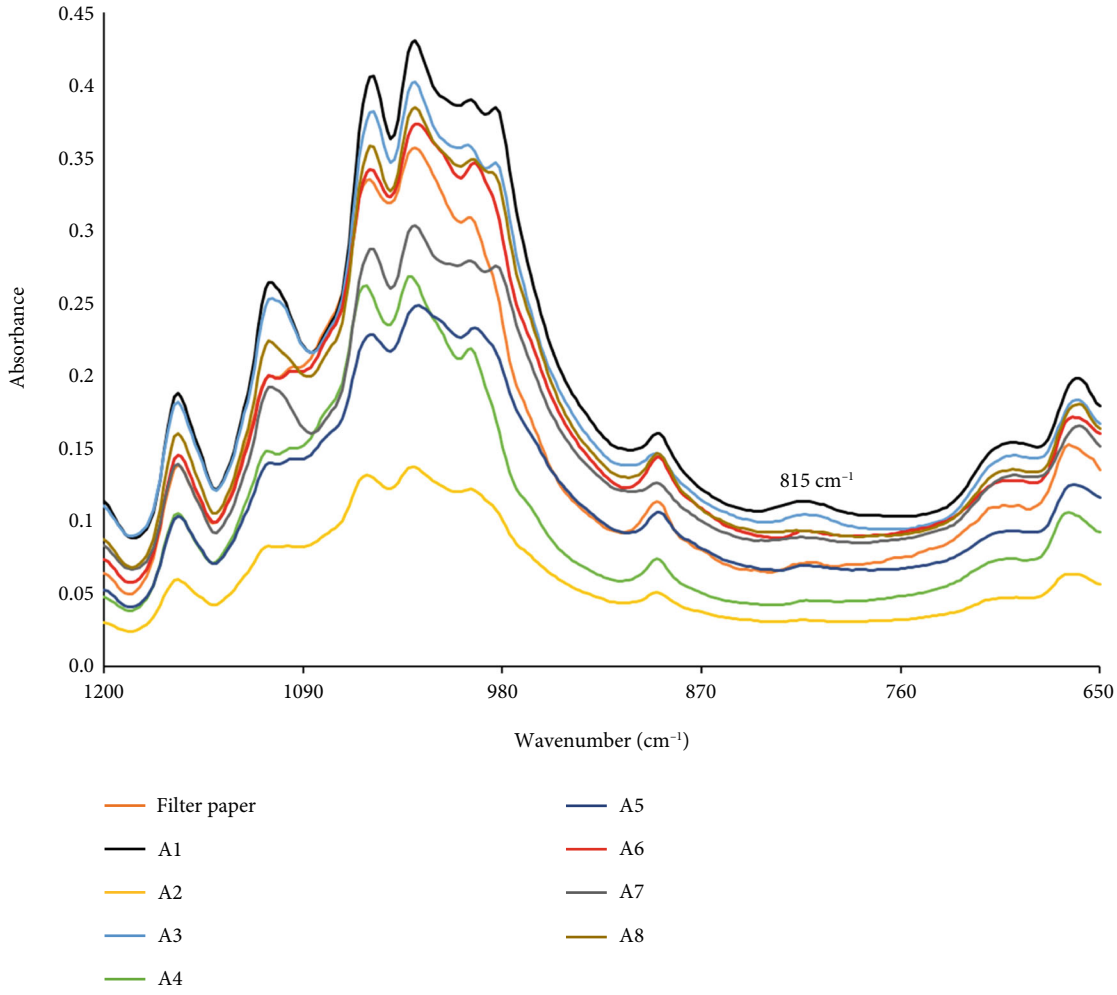

Figure 4: FTIR spectra of CNC samples in the 1200–650 cm^{-1} range.

temperature caused a higher content of sulfate groups on the sample.

Figure 5(b) shows the first derivative of the degradation curve, this figure helps to identify the starting point of the degradation of samples. In Figure 5(b), the TGA results can be confirmed. Samples A1 and A3 have a slow degradation speed. The complex degradation behavior is seen as a primary degradation peak at 150°C, and several secondary peaks, among them, a peak at 380°C. On the other hand, sample A2 has a higher thermal degradation speed, with a peak at 325°C. Samples A4 and A5 have also fast speeds of degradation, without secondary degradation peaks.

3.3. X-Ray Diffraction. The calculated crystallinity indices (CrI) of the CNC samples are shown in Table 2. The CrIs are not very high, the highest calculated CrI is 64.72%. In Table 2, it is observed that the lowest CrI corresponds to a sample synthesized at 30 minutes, 64 wt% H_2SO_4, and 45°C. This sample is followed by the one obtained at 30 minutes, 30 wt% H_2SO_4, and 80°C. These results might be due to a lower reaction time, shortening the reaction of decomposition of the amorphous parts; the latter sample with the higher crystallinity was synthesized at a higher temperature; the samples mentioned above were synthesized with more acid, but with less time and temperature. Finally, the higher CrI average corresponds to samples synthesized at 60 minutes, 30 wt% H_2SO_4, and 45°C, these samples were synthesized with more reaction time, low acid content, and a low temperature. These conditions were favorable for the hydrolysis conditions of the amorphous parts by the sulfuric acid, and the observed higher crystallinity is similar to previous works found in the literature [20]. On the other hand, the sample synthesized with harsher conditions, such as 60 minutes, 64 wt% of acid, and 80°C, had a high crystallinity but lower than the samples mentioned above, this may be due to the high temperature, which causes dehydration of CNCs.

Figure 6 shows the powder diffractograms of the CNC samples synthesized under different conditions. All the samples have the characteristic reflections of CNC in similar positions, but the low CrI makes some reflections look convoluted. The observed peaks on the samples are (1–10) at 15.7°, (110) at 20.1°, (200) at 22.8°, and (004) at 36.9°. It is reported in the literature that the major crystalline peaks of CNC are located before 35° [27]. Figure 5 shows the diffractogram of filter paper, given for comparison between the diffractograms of the raw material and that of the CNC

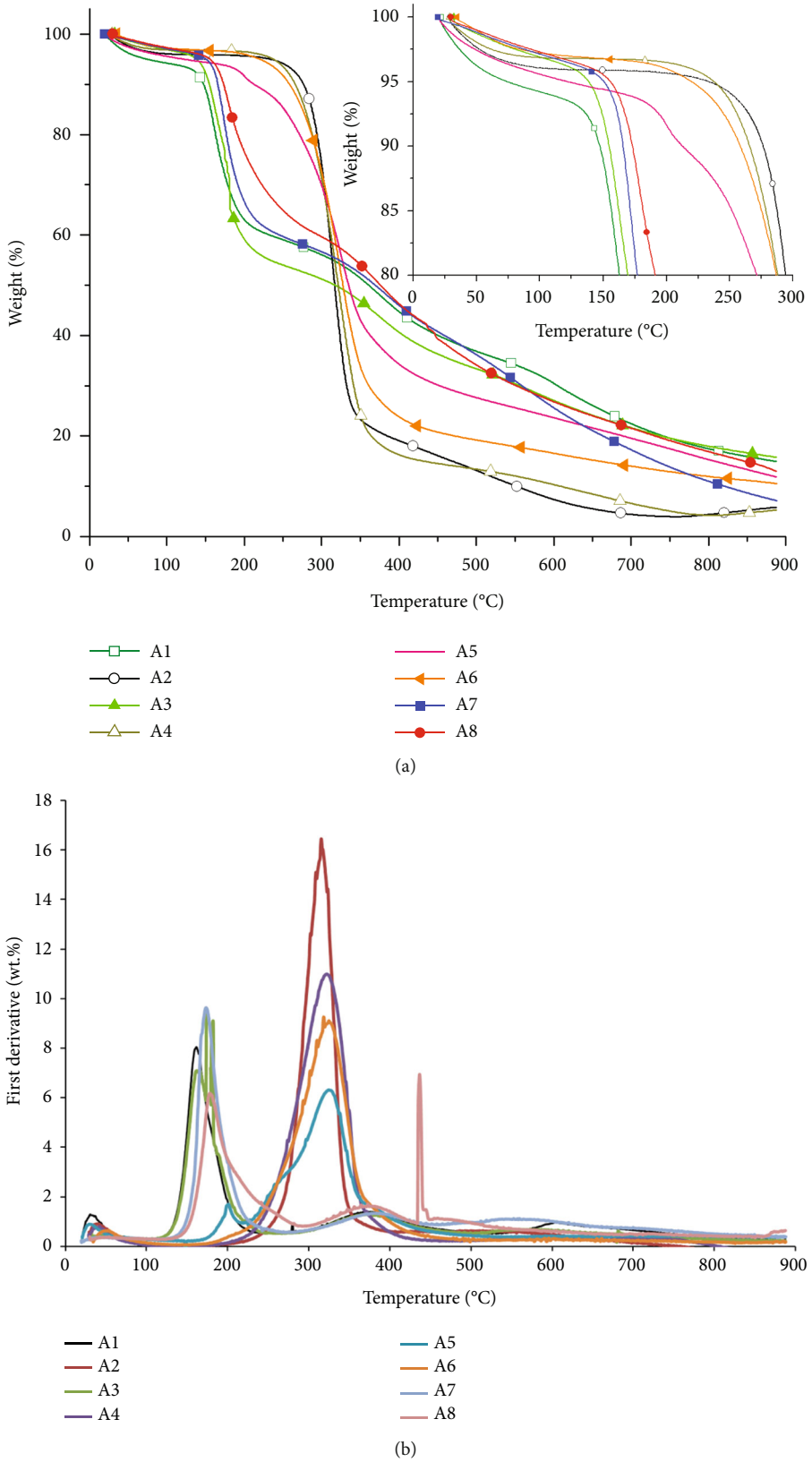

Figure 5: (a) Thermogram curves of CNC samples. (b) The first derivative of thermograms.

Table 2: CrI of the CNC samples.

Time (minutes)	H_2SO_4 (wt%)	T (°C)	Name	CrI (%)	Crystallite size
30	30	80	A1	59.22	4.02
60	64	80	A2	62.13	3.92
30	64	45	A3	60	3.22
60	30	45	A4	64.72	3.88
30	30	80	A5	60.07	3.87
60	64	80	A6	61.35	3.99
60	30	45	A7	64.17	3.63
30	64	45	A8	57.72	3.70

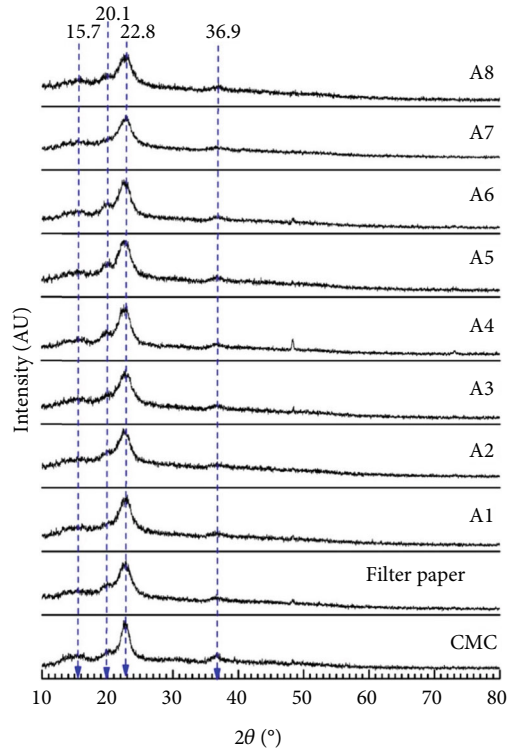

Figure 6: XRD powder diffractograms of CNC samples.

samples. The diffractogram of filter paper has the (200) reflection at 23°, next to it, there is an amorphous halo centered approximately at 20°; this halo is also present to a lesser degree in some samples, such as A5. The diffractogram is characteristic of amorphous polysaccharides, and filter paper has a CrI of 51.64%, this indicates that the CrI of CNC samples was increased after the hydrolysis with sulfuric acid. Figure 6 includes the diffractogram of commercial CMC shown for comparison. The diffractogram of CMC is typical of cellulosic samples and is similar to the diffractograms of the CNCs and filter paper.

The crystallite sizes of the CNC samples are shown in Table 2. The average crystallite size is 3.78 ± 0.26 nm. This value is similar to the crystallite size obtained by authors in the literature when agro-industrial wastes are used as cellulose sources [28], and they are smaller than the average crystallite size reported in the literature [29]. Chain rearrangement of cellulose causes a change in cellulose polymorphs, and it leads to a change in crystallinity [23]; in the case of the formation of cellulose III, there is a decrease in crystallinity. However, the XRD reported in this study suggests that the polymorph corresponds to cellulose I, and the process for cellulose purification and CNC extraction does not lead to the formation of cellulose III. It has been reported in literature [23], that lower crystallinity of CNCs leads to a smaller crystallite size. Then, the observed low crystallinity of CNCs observed in this study correlates with the small calculated crystallite size.

3.4. Atomic Force Microscopy. The nanocrystals were observed by AFM, this technique allows an accurate observation of nanoparticles in colloidal suspensions [30]. The nanocrystals had a rod-like shape, with the agglomeration of the nanocrystals. Figure 7(a) shows an AFM image of the nanocrystals of sample A7, this sample was chosen as it was the most representative of the CNC samples, other samples showed aggregation or incomplete hydrolysis. The TGA of sample A7 suggested that it has more sulfate content than that of other samples, the sulfate on the CNC samples influences the morphology of the sample. The sample was diluted by a factor of 50. They have a rod-like shape, with a lot of aggregation of the nanocrystals. Figure 7(b) also shows an AFM image of the diluted nanocrystals but with a higher magnification. The sample was diluted by a factor of 200, four times the dilution factor of the original nanocrystals. The measured dimensions were 436.5 ± 18 nm in length and 102.6 ± 2.3 nm in diameter. The large diameter may be due to the agglomeration of CNCs, this material tends to aggregate in parallel [31]; in addition, it is reported in the literature that AFM has poor lateral resolution, whereas it is good for measuring height [31]. The shape of the nanocrystals and the observed aggregation is comparable with the characteristics of CNC samples observed in the literature [30, 32, 33]. Figure 8(a) shows the AFM micrograph of sample A8 with a scale of 20 μm, and Figure 8(b) shows the sample with a scale of 3 μm. The dilution factor was 50. The nanocrystals have a rod-like shape, they look similar to the nanocrystals of sample A7. The images show aggregation of the nanocrystals. The CNC of sample A8 measured 200.3 ± 7.7 nm in length and had a diameter of 42.9 ± 1.3 nm. The L/D ratio was 4.25 for the A7 sample and 4.67 for the A8 sample. The L/D ratio of these samples is in the smaller range of reported values [34, 35], this is attributed to the aggregation of the samples.

Figure 9 shows the height profile of all the samples, it was obtained by the Gwyddion software. The height distribution of most samples is narrow, except for sample A5 (time = 30 minutes, concentration = 30 wt%, and $T = 80$°C). The narrow height distribution calculated by the Gwyddion software is similar to the size distribution calculated manually for the aforementioned samples (±2.3 nm for A7 and ±1.3 nm for A8), similar results have been found in the literature [25]; whereas in some works, it is assumed that the height of the nanocrystals is equal to their diameter [32]; although, it is reported in some works that the height does

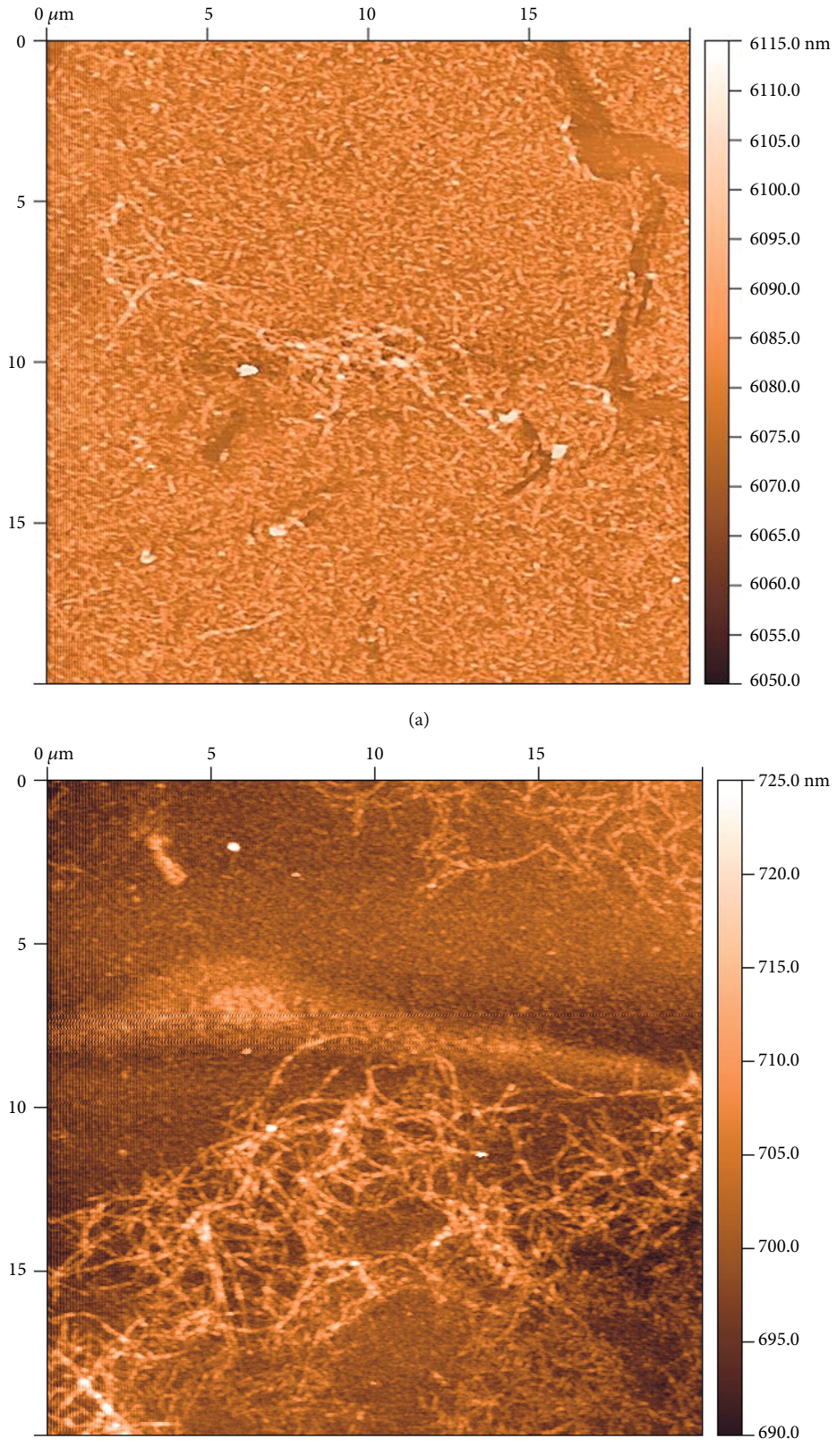

Figure 7: AFM micrograph of sample A7. Scale: 20 μm. (a) Undiluted sample. (b) Diluted sample.

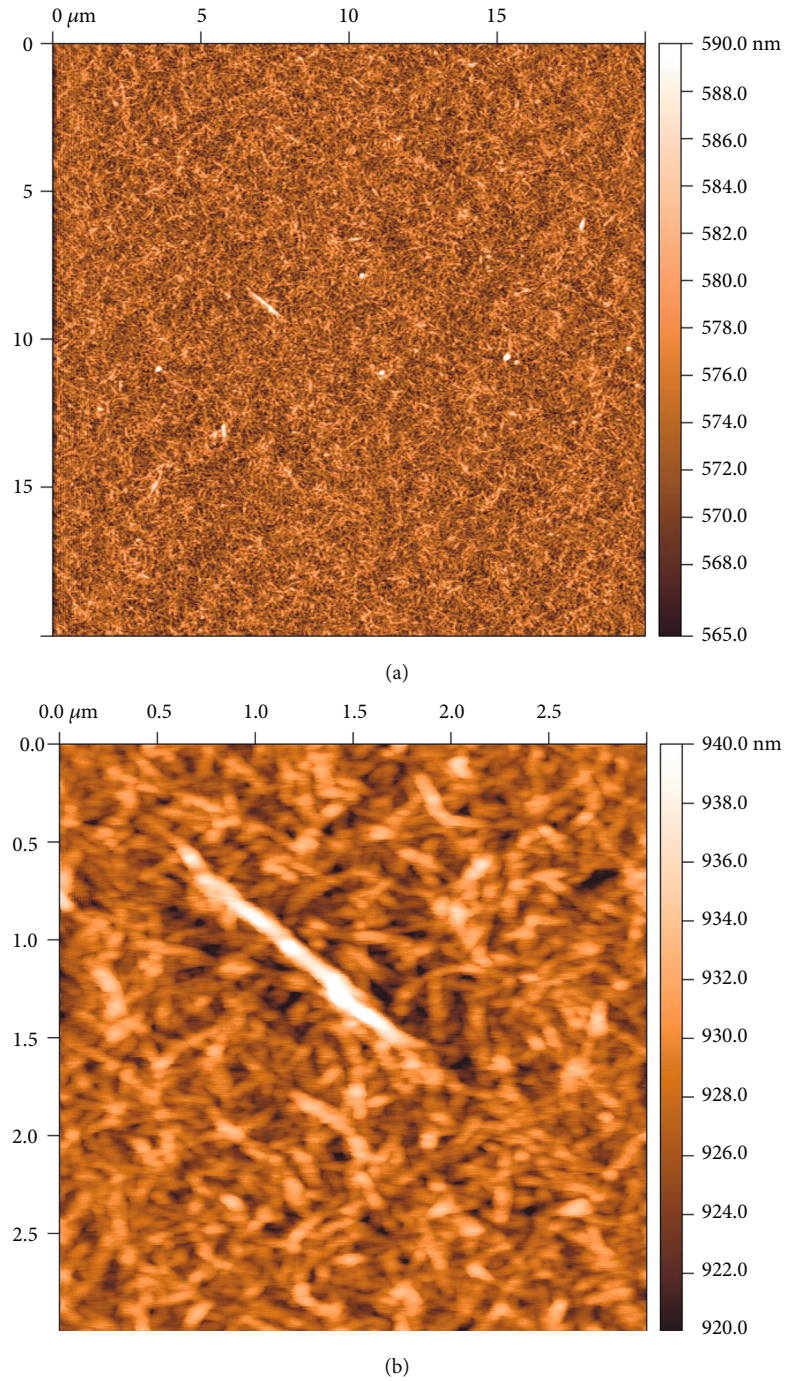

Figure 8: AFM micrograph of sample A8. (a) Scale: 20 μm. (b) Scale: 3 μm.

not correspond to the width of CNCs [36]. In our work, the measured height is lower than the measured width. Table 3 summarizes the height and distribution height of the samples. The smaller heights correspond to samples A6, A4, and A8. The highest value is that of the sample A2.

3.5. Analysis of Results. With the results obtained by FTIR, TGA, XRD, and AFM, it can be inferred that the reaction conditions influence the sulfate content, as reported in the literature [20, 21, 37]. The sulfuric acid attacks the amorphous parts of cellulose, releasing the crystalline parts, and introducing sulfate groups on the surface of the sample [20, 37]. The TGA suggested that some samples had lower sulfate content, whereas some had higher sulfate content. This parameter depended on the reaction conditions [20, 37]. The samples synthesized at the lower conditions of variables had lower sulfate content; whereas the samples with higher conditions of variables had higher sulfate content [37]. Harsher conditions lead to sulfuric acid attacking the crystalline parts [18], thus leading to shorter crystals [37], and, if the concentration or

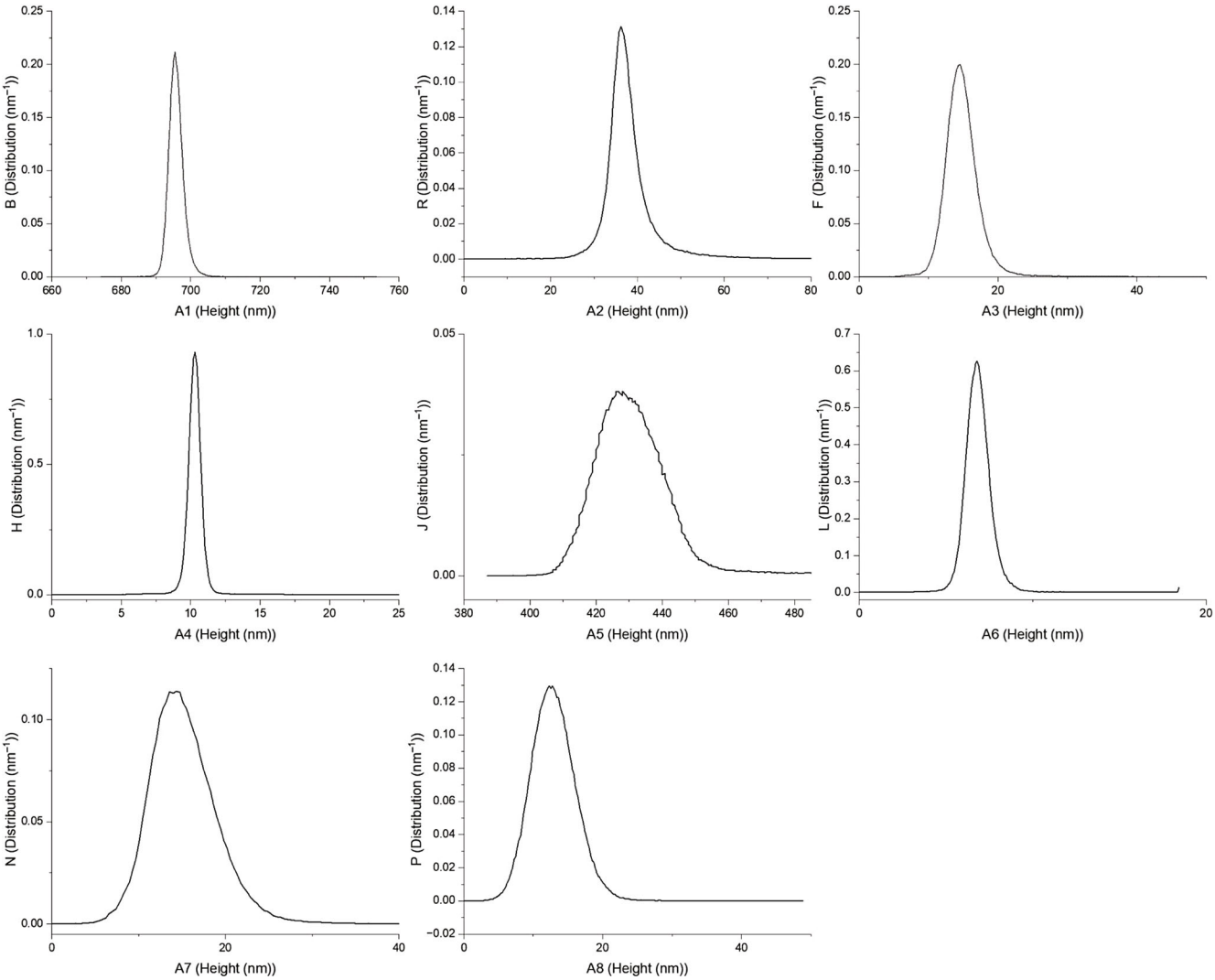

Figure 9: Height profiles and the distribution of the samples.

Table 3: Height and distribution of the samples.

Sample	Height (nm)	Distribution (nm^{-1})
A1	13.55	0.159
A2	36.45	0.130
A3	14.58	0.199
A4	10.28	0.916
A5	37.42	0.380
A6	6.81	0.623
A7	14.24	0.113
A8	12.39	0.128

the temperature is too high, to carbonization of cellulose. FTIR and TGA showed that the variables influenced the sulfate content, and all three variables had different effects. As stated above, milder conditions led to lower sulfate content, whereas harsher conditions led to higher sulfate content. Figure 10 shows a scheme summarizing the process. In Figure 11, the intermediate conditions refer to 30 minutes of reaction, 64 wt% of H_2SO_4, and 45°C, close to the published values for optimum CNC extraction of 45 minutes, 64 wt% of H_2SO_4, and 45°C [20].

3.6. Supercapacitors. The samples A3 and A8 (30 minutes, 64 wt%, and 45°C) showed the best results in characterization. These results are in line with previous works [20, 37]. As the reaction parameters were close to the traditional synthesis of CNCs, described in the literature [20], we used CNCs fabricated in that way for an experiment, the details of the synthesis can be found in the literature [14]. The CNCs were used as binders in electrodes. The electrodes were made with graphite-doped activated carbon (AC/C). Without CNCs, the electrode tablet crumbled. The stability of the tablet increased with CNC addition, starting from an easily crumbling tablet, until a stable tablet was formed with increased content of the CNCs. Figure 1 shows the cell where the tests were done, this cell was tightly closed to minimize air presence. The curves of voltammetry (CV) are shown in Figure 11. The curves are quasi-quadrangular, showing a capacitor-like behavior. Curves improved at

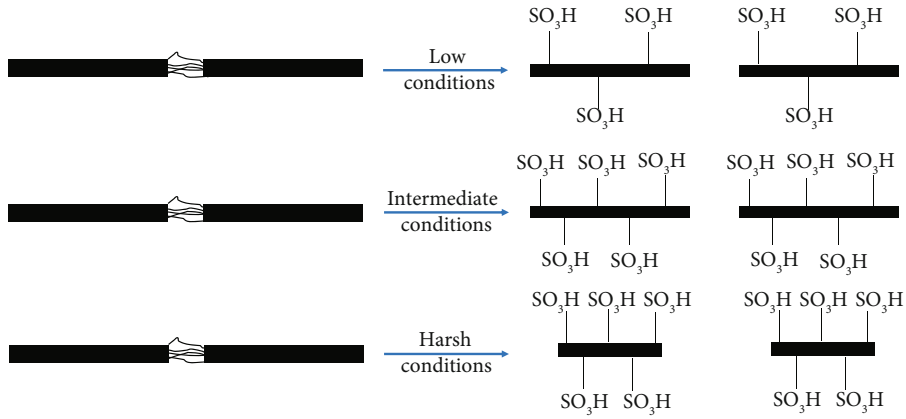

Figure 10: Scheme summarizing the process of CNC production.

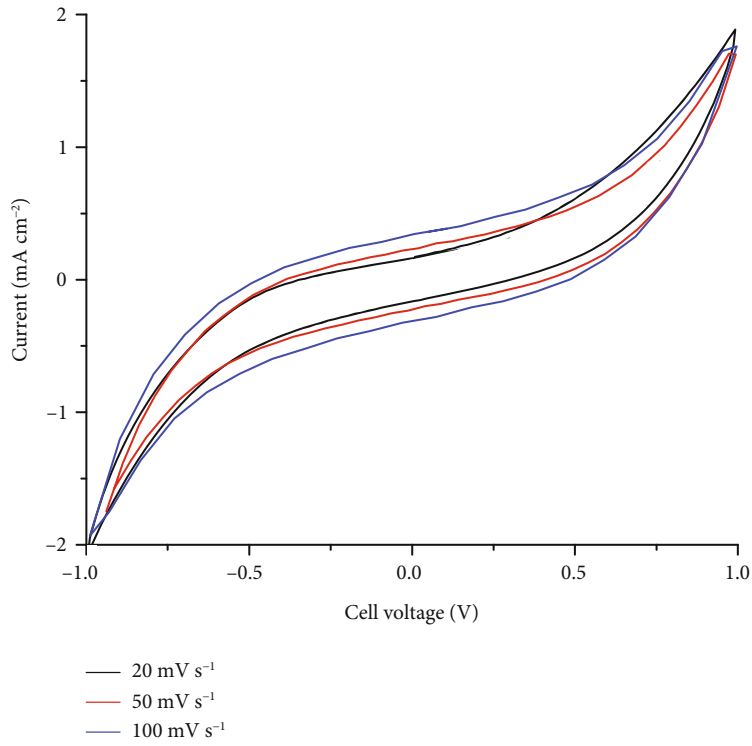

Figure 11: CV voltammograms of the AC/C electrodes with CNCs as a binder. Symmetric capacitor.

higher scan rates, agreeing with similar works [38]. However, the area/speed factor is lower at the higher scan rates than at the lower scan rates. These results showed that CNCs can be used as binders in electrode capacitors, as CNFs, which are currently used [5].

The voltammograms showed a quasi-rectangular shape. This behavior is reported that is due to the good capacitive nature of this symmetric capacitor [39]. Furthermore, the voltammograms without distinct redox peaks at the test rates indicate that it is only the electromotive force between Na+ and OH− ions of the electrolyte and the carbon electrodes [40]. At 100 mV s^{-1}, the largest current area was observed compared with the other rates, which is attributed to the improved charge storage capacity at that rate [41]. In this study, we have prepared a device based on activated carbon, graphite, and CNCs using KOH as an electrolyte. To determine if the device functioned as a capacitor, a cell voltage window of −1 to 1 V was used. However, this voltage window was wide, affecting the characteristic rectangular shape of a symmetrical capacitor. Using a potential window of −0.5 to 0.5 V and 100 mV s^{-1}, for example, the voltammogram shape would be substantially improved. In addition, the distortion from the classic shape of the capacitor could be attributed to pseudocapacitance caused by the quasi-reversible surface reactions and the limitation in the charge transfer imposed by the narrow micropores [42].

The C_{CV} data at different scan rates are 35.93 F g^{-1} (20 mV s^{-1}), 19.07 F g^{-1} (50 mV s^{1}), and 14.26 F g^{-1} (100 mV s^{-1}).

This value is lower than those of asymmetric supercapacitors obtained from treated activated carbon from anthracite, using polytetrafluoroethylene (PTFE) as a binder and 0.5 M Na_2SO_4 as an electrolyte, with a capacitance of 67–166 F g^{-1} obtained [43]. It is also lower than the capacitance of supercapacitors fabricated with activated carbon and graphene nanoplatelets, using PTFE as a binder; in this case, the capacitance was calculated with values of 51.77–109.75 F g^{-1} [44]. The capacitance influences the electrical resistivity of the material, that is, the higher the capacitance, the lower its electrical resistivity. Likewise, electrical resistivity can affect capacitance, the higher the electrical resistivity, the lower its ability to store electrical energy. CNCs have a lower capacitance compared with PTFE because it most likely has a higher electrical resistivity. In addition, other factors that affect the ability to store energy are cross-sectional area; the larger the cross-sectional area, the lower the electrical resistance, since electrons have a larger area to flow and vice versa, the smaller the cross-sectional area, the greater the electrical resistance. An increase in temperature causes the particles to vibrate more, and the electrical conductivity decreases because molecules are more likely to get in the way of current flow. Likewise, moisture in the material allows more electrical current to flow, which increases the capacitance of the capacitor. These factors can influence the capacitance values of CNCs and PTFE.

For the AC/C devices; when the scan rate is increased, the C_{CV} decreased. This behavior could be because the electrolyte ions have more time to diffuse from the solution to the pores of the electrode at a low scan rate [45]. The values obtained for C_{CV} show that CNCs can be used as a binder for the manufacture of electrodes for capacitors. However, more studies are required to obtain a better performance in the devices.

The CNCs stabilized the AC/C electrodes, forming a network between the AC/C and CNC via π–π stacking interaction with no covalent bonding [46], as activated carbon and CNF are stabilized by this kind of interaction [46, 47]. The network and its interaction are shown in Figure 12, the activated carbon of the AC/C electrode was modelled after the results of Allen et al. [48]. Capacitors and supercapacitors using CNF as binders have been widely reported in the literature [5, 49, 50], in those devices, CNF stabilizes the electrodes and prevents crumbling; however, CNCs have not been reported as binders for capacitors and supercapacitors, they have been used as flexible dielectric paper [7], as dielectric paper immersed in oil transformer, where they showed a dielectric strength higher than normal commercial paper [51], and in supercapacitors as dielectric material [38]. In this study, we used successfully CNCs as binders in a capacitor device.

3.7. Electrochemical Impedance Spectroscopy. The EIS analysis of activated carbon doped with graphite (AC/C) and CNCs suspension as binder was studied in a two-electrode cell and it was carried out to understand the processes that are taking place at the electrode/electrolyte interface, and a new device was used for this analysis. The Nyquist plot in

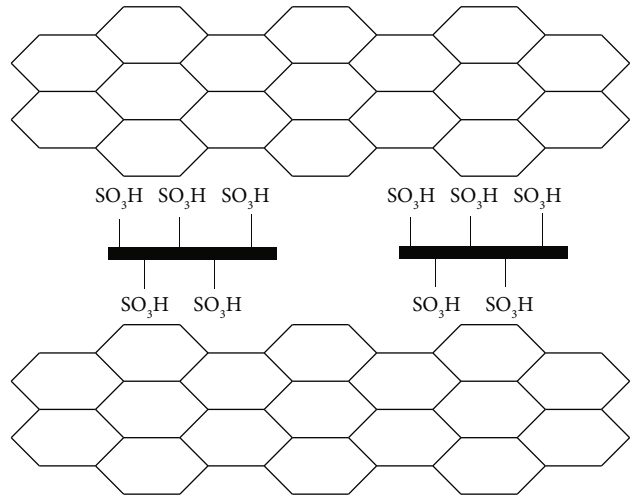

Figure 12: AC/C–CNC network.

Figure 13 shows a semicircle at high frequencies (HF) and a small straight line at low frequencies (LF). The possible causes of the semicircle in HF are the porous structures of AC/C–CNCs electrode with a complex network of distributed capacitive/resistive components and the kinetic leakage processes arising from interfacial oxidation–reduction reactions of impurities and surface functionalities of carbons [52]. The inclined 45° line at LF is characteristic of transmission-line-like behavior, attributing to the impedance correlating with the distributed resistance/capacitance in the AC electrodes [53, 54]. In this case, the line is inclined at an angle less than 45°, indicating that a resistive behavior predominates or that the LF was not low enough to be able to observe the capacitive behavior. The equivalent series resistance (includes the resistance of the electrolyte, intrinsic resistance of the materials, contact resistance between the materials, and contact resistance between the anode/cathode and the current collectors) [55] of AC/C with CNCs was 14.69 Ω. In a study [56], styrene–butadiene rubber and PTFE were used as a binder. ESRs of the order of 10^{-1} were reported indicating that the binder had an adhesion that allowed better contact between the activated carbon and the current collector with less clogging of the pores in the activated carbon and better wetting of the electrolyte. This binder behavior contributed to lower resistances in the EIS analysis. In our case, the ESR obtained is one order of magnitude higher compared with SRB/PTFE, indicating that our binder could have poor adhesion and allowed a greater number of pores available in the process.

The main parameters from the EIS are given in Table 4. The phase coefficient and the CPE element can be interpreted as an ideal capacitor ($n = 1$) or a resistor ($n = 0$). In this case, the n value was 0.76. The fitted EIS data are shown in Figure 13, and the error % was lower than 4.

4. Conclusions

Acid hydrolysis of cellulose was performed under different parameters. Sulfate groups were introduced on the surface of cellulose nanocrystals. FTIR and TGA suggested that the

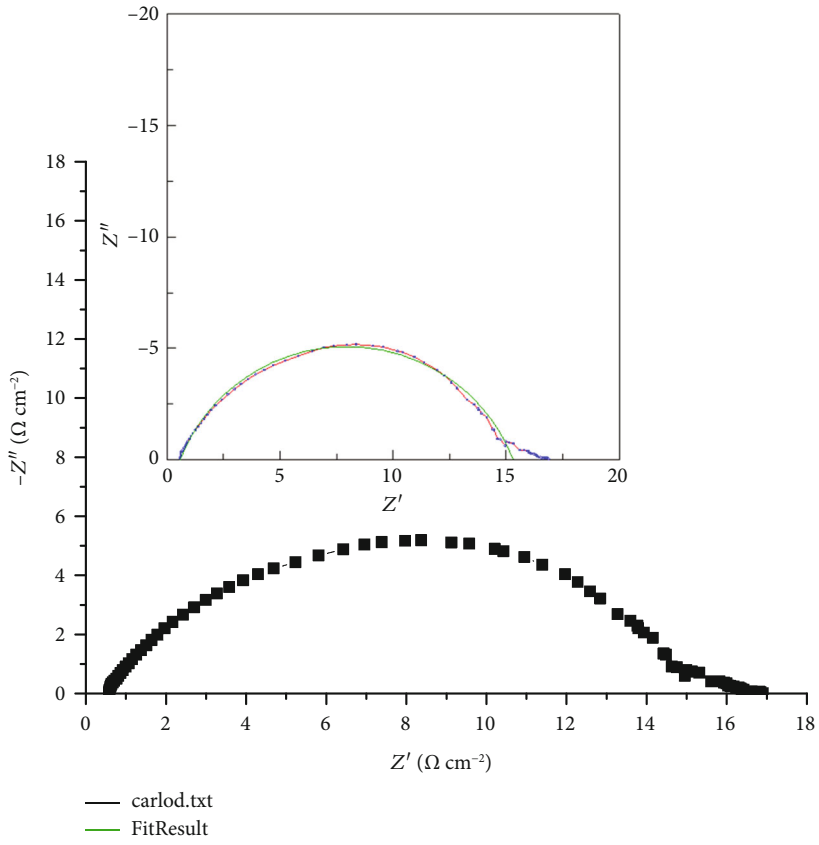

Figure 13: Nyquist plot for prepared device and fitted EIS data.

Table 4: Values of the main parameters from the EIS.

	R_s (Ω cm^{-2})	CPE (s^n Ω^{-1} cm^{-2})	n	R_{ct} (Ω cm^{-2})
AC/C–CNCs	0.68	2.8×10^{-4}	0.76	14.01

sulfate content on the surface of CNCs varied ranging from low content to high content. FTIR characterization showed that the CNC samples have the characteristic functional groups of cellulose, and the bands present on the spectra resemble the bands found in the literature for CNCs. FTIR suggested that CNC samples are crystalline and are composed of the polymorph I of cellulose, which is the polymorph found in plants. Thermal degradation of samples indicated that the reaction conditions influenced the sulfate content of the CNC samples. The samples with a high speed of thermal degradation suggested a low sulfate content, as their thermal degradation resembled that of cellulose, whereas the samples with a low speed and complex thermal degradation suggested a high sulfate content, as their degradation behavior is more complex and sulfate groups are thermally unstable. FTIR and TGA results agreed on the sulfate content of the samples. XRD showed an increase in the crystallinity of the samples after hydrolysis of acid as seen in comparison with the diffractogram of pure cellulose, which showed an amorphous halo. The crystallite size in this study was smaller than the average size reported in the literature, and the best conditions for the synthesis of CNCs are 30 minutes, 64 wt% of H_2SO_4, and 45°C. CNCs can be used as binders of electrodes in symmetric capacitors based on activated carbon, as CNFs are also used. The amount of CNCs needed to give cohesion to the electrodes is very small. CNCs did not interfere with the electrical charge of the electrodes, cyclic voltammograms showed a quasi-rectangular shape indicating the potential of CNCs for energy storage applications.

Data Availability

Data supporting this research article are available from the corresponding author or first author upon reasonable request.

Conflicts of Interest

The author(s) declare(s) that they have no conflicts of interest.

Acknowledgments

The authors want to acknowledge Consejo Nacional de Humanidades, Ciencia y Tecnología (CONAHCyT) for funding this project with grant number 283518.

References

[1] A. Sharma, M. Thakur, M. Bhattacharya, T. Mandal, and S. Goswami, "Commercial application of cellulose nanocomposites—a review," *Biotechnology Reports*, vol. 21, article e00316, 2019.

[2] P. Phantong, P. Reubroycharoen, X. Hao, G. Xu, A. Abudula, and G. Guan, "Nanocellulose: extraction and application," *Carbon Resources Conversion*, vol. 1, no. 1, pp. 32–43, 2018.

[3] S. Pereira, M. Pronk, J. Zlopasa, S. J. Picken, and M. C. M. van Loosdrecht, "Nanocellulose recovery from domestic wastewater," *Journal of Cleaner Production*, vol. 280, article 124507, 2021.

[4] D. G. Gray, "Cellulose nanocrystal research; a personal perspective," *Carbohydrate Polymers*, vol. 250, article 116888, 2020.

[5] A. H. Tayeb, E. Amini, S. Ghasemi, and M. Tajvidi, "Cellulose nanomaterials-binding properties and applications: a review," *Molecules*, vol. 23, p. 2684, 2018.

[6] B.-R. Lee and E.-S. Oh, "Effect of molecular weight and degree of substitution of a sodium-carboxymethyl cellulose binder on Li4Ti5O12 anodic performance," *Journal of Physical Chemistry C*, vol. 117, no. 9, pp. 4404–4409, 2013.

[7] R. Koppolu, T. Abitbol, V. Kumar, A. K. Jaiswal, A. Swerin, and M. Toivakka, "Continuous roll-to-roll coating of cellulose nanocrystals onto paperboard," *Cellulose*, vol. 25, no. 10, pp. 6055–6069, 2018.

[8] T. K. Saha and P. Purkait, "Transformer insulation materials and ageing," in *Transformer Ageing*, T. K. Saha and P. Purkait, Eds., pp. 1–4, Wiley, Singapore, 2017.

[9] D. Le Bras, M. Strömme, and A. Mihranyan, "Characterization of dielectric properties of nanocellulose from wood and algae for electrical insulator applications," *The Journal of Physical Chemistry B*, vol. 119, no. 18, pp. 5911–5917, 2015.

[10] V. Pakharenko, J. Sameni, S. Konar et al., "Cellulose nanofiber thin-films as transparent and durable flexible substrates for electronic devices," *Materials and Design*, vol. 197, article 109274, 2021.

[11] P. Panchal, E. Ogunsona, and T. Mekonnen, "Trends in advanced functional material applications of nanocellulose," *Processes*, vol. 7, p. 10, 2018.

[12] T. Chen, X. He, T. Jian et al., "Synthesis and drug delivery properties of ibuprofen-cellulose nanofibril system," *International Journal of Biological Macromolecules*, vol. 182, pp. 931–937, 2021.

[13] C. F. Castro-Guerrero and D. G. Gray, "Chiral nematic phase formation by aqueous suspensions of cellulose nanocrystals prepared by oxidation with ammonium persulfate," *Cellulose*, vol. 21, no. 4, pp. 2567–2577, 2014.

[14] C. F. Castro-Guerrero, A. B. Morales-Cepeda, M. R. Díaz-Guillén, F. Delgado-Arroyo, and F. A. López-González, "Self-ordered cellulose nanocrystals and microscopic investigations," *Materials Science-Poland*, vol. 38, no. 4, pp. 613–618, 2020.

[15] W. Zhang, Y. Tan, Y. Gao, J. Wu, B. Tang, and J. Zhao, "Amorphous nickel-boron and nickel-manganese-boron alloy as electrochemical pseudocapacitor materials," *RSC Advances*, vol. 4, no. 53, pp. 27800–27804, 2014.

[16] I. Ahamad, R. Prasad, and M. A. Quraishi, "Adsorption and inhibitive properties of some new Mannich bases of Isatin derivatives on corrosion of mild steel in acidic media," *Corrosion Science*, vol. 52, no. 4, pp. 1472–1481, 2010.

[17] C. Y. Liang and R. H. Marchessault, "Infrared spectra of crystalline polysaccharides. I. Hydrogen bonds in native celluloses," *Journal of Polymer Science*, vol. 37, no. 132, pp. 385–395, 1959.

[18] M. L. Nelson and R. T. O'Connor, "Relation of certain infrared bands to cellulose crystallinity and crystal latticed type. Part I. Spectra of lattice types I, II, III and of amorphous cellulose," *Journal of Applied Polymer Science*, vol. 8, no. 3, pp. 1311–1324, 1964.

[19] F. Shafizadez and A. G. W. Bradbury, "Thermal degradation of cellulose in air and nitrogen at low temperatures," *Journal of Applied Polymer Science*, vol. 23, no. 5, pp. 1431–1442, 1979.

[20] X. M. Dong, J.-F. Revol, and D. G. Gray, "Effect of microcrystallite preparation conditions on the formation of colloid crystals of cellulose," *Cellulose*, vol. 5, pp. 19–32, 1998.

[21] J. H. Jordan, M. W. Easson, and B. D. Condon, "Alkali hydrolysis of sulfated cellulose nanocrystals: optimization of reaction conditions and tailored surface charge," *Nanomaterials*, vol. 9, no. 9, p. 1232, 2019.

[22] F. Delgado-Arroyo, C. F. Castro-Guerrero, and U. León-Silva, "Thin films of cellulose acetate nanofibers from cigarette butt waste," *Progress in Rubber, Plastics and Recycling Technology*, vol. 2020, no. 36, pp. 3–17, 2020.

[23] J. Gong, J. Li, J. Xu, Z. Xiang, and L. Mo, "Research on cellulose nanocrystals produced from cellulose sources with various polymorphs," *RSC Advances*, vol. 7, no. 53, pp. 33486–33493, 2017.

[24] F. Hemmati, S. M. Jafari, and R. A. Taheri, "Optimization of homogenization-sonication technique for the production of cellulose nanocrystals from cotton linter," *International Journal of Biological Macromolecules*, vol. 137, no. 137, pp. 374–381, 2019.

[25] E. U. Pulido-Barragán, C. F. Castro-Guerrero, A. M. Zamudio, A. B. Morales-Cepeda, T. Heinze, and A. Koschella, "Isolation of cellulose nanocrystals from Typha domingensis named southern cattail using a batch reactor," *Fibers and Polymers*, vol. 20, no. 6, pp. 1136–1144, 2019.

[26] M. Thakur, A. Sharma, V. Ahlawat, M. Bhattacharya, and S. Goswami, "Process optimization for the production of cellulose nanocrystals from rice straw derived α-cellulose," *Materials Science for Energy Technologies*, vol. 3, pp. 328–334, 2020.

[27] X. Ju, M. Bowden, E. E. Brown, and X. Zhang, "An improved X-ray diffraction method for cellulose crystallinity measurement," *Carbohydrate Polymers*, vol. 123, pp. 476–481, 2015.

[28] H. Kargarzadeh, M. Loelovich, I. Ahmad, S. Y. Thomas, and A. Dufresne, "Methods for extraction of nanocellulose from various sources," in *Handbook of Nanocellulose and Cellulose Nanocomposites*, H. Kargarzadeh, I. Ahmad, S. Thomas, and A. Dufresne, Eds., pp. 1–49, Wiley, Weinheim, Germany, 2017.

[29] M. G. Aguayo, A. Fernández-Pérez, C. Oviedo, G. Reyes, and P. Reyes-Contreras, "Relationship between structural characteristics of cellulose nanocrystals obtained from Kraft pulp," *Nanomaterials*, vol. 10, no. 9, p. 1775, 2020.

[30] T. Abitbol, E. Kloser, and D. G. Gray, "Estimation of the surface sulfur content of cellulose nanocrystals prepared by sulfuric acid hydrolysis," *Cellulose*, vol. 20, no. 2, pp. 785–794, 2013.

[31] L. C. E. da Silva, A. Cassago, L. Battirola, M. do Carmo Goncalves, and R. V. Portugal, "Specimen preparation

optimization for size and morphology characterization of nanocellulose by TEM," *Cellulose*, vol. 27, no. 9, pp. 5435–5444, 2020.

[32] M. Chen, J. Parot, V. A. Hackley, S. Zou, and L. J. Johnston, "AFM characterization of cellulose nanocrystal height and width using internal calibration standards," *Cellulose*, vol. 28, no. 4, pp. 1933–1946, 2021.

[33] L. Douard, J. Bras, T. Encinas, and M. N. Belgacem, "Natural acidic deep eutectic solvent to obtain cellulose nanocrystals using the design of experience approach," *Carbohydrate Polymers*, vol. 252, article 117136, 2021.

[34] A. Pei, J.-M. Malho, J. Ruokolainen, Q. Zhou, and L. A. Berglund, "Strong nanocomposite reinforcement effects in polyurethane elastomer with low volume fraction of cellulose nanocrystals," *Macromolecules*, vol. 44, no. 11, pp. 4422–4427, 2011.

[35] R. Olmos-Juste, B. Alonso-Lerma, R. Pérez-Jiménez, N. Gabilondo, and A. Eceiza, "3D printed alginate-cellulose nanofibers based patches for local curcumin administration," *Carbohydrate Polymers*, vol. 264, article 118026, 2021.

[36] N. Shahmiri, N. H. Nemati, A. R. Saadatabadi, and M. Seifi, "Cellulose nanocrystal (CNC) synthesis: an AFM study," *Journal of Nanostructures*, vol. 11, p. 684, 2021.

[37] K.-H. Lin, T. Enomae, and F.-C. Chang, "Cellulose nanocrystal isolation from hardwood pulp using various hydrolysis conditions," *Molecules*, vol. 24, no. 20, p. 3724, 2019.

[38] J. A. Hernández-Flores, A. B. Morales-Cepeda, C. F. Castro-Guerrero et al., "Morphological and electrical properties of nanocellulose compounds and its application on capacitor assembly," *International Journal of Polymer Science*, vol. 2020, p. 1891014, 2020.

[39] R. Suresh, K. Tamilarasan, and D. S. Vadivu, "Electrochemical features of symmetric and asymmetric supercapacitors based on nanostructured Mn-CuO electrodes," *Oriental Journal of Chemistry*, vol. 34, no. 6, pp. 3058–3063, 2018.

[40] D. Kasprzak, I. Stepniak, and M. Galinski, "Electrodes and hydrogel electrolytes based on cellulose: fabrication and characterization as EDLC components," *Journal of Solid State Electrochemistry*, vol. 22, no. 10, pp. 3035–3047, 2018.

[41] Y. Liu, Z. Hu, K. Xu, X. Zheng, and Q. Gao, "Surface modification and performance of activated carbon electrode material," *Acta Physico-Chimica Sinica*, vol. 24, no. 7, pp. 1143–1148, 2008.

[42] R. Farma, M. Deraman, A. Awitdrus et al., "Preparation of highly porous binderless activated carbon electrodes from fibres of oil palm empty fruit bunches for application in supercapacitors," *Bioresource Technology*, vol. 132, pp. 254–261, 2013.

[43] I. Piñeira-Prado, D. Salinas-Torres, R. Ruiz-Rosas, E. Morallón, and D. Cazorla-Amorós, "Design of activated carbon/activated carbon asymmetric capacitors," *Frontiers in Materials*, vol. 3, p. 3, 2016.

[44] A. H. A. Rahim, N. Ramli, A. N. Nordin, and M. F. A. Wahab, "Supercapacitor performance with activated carbon and graphene nanoplatelets composite electrodes, and insights from the equivalent circuit model," *Carbon Trends*, vol. 5, article 100101, 2021.

[45] W. Wang, K. Li, G. Song, M. Zhou, and P. Tan, "Activated carbon aerogel as an electrode with high specific capacitance for capacitive deionization," *PRO*, vol. 10, no. 11, p. 2330, 2022.

[46] A. Sobhan, K. Muthukumarappan, Z. Cen, and L. Wei, "Characterization of nanocellulose and activated carbon nanocomposite films' biosensing properties for smart packaging," *Carbohydrate Polymers*, vol. 225, article 115189, 2019.

[47] M. Wu, M. Wang, and M. Ge, "Investigation into the performance and mechanism of SiO2 nanoparticles and starch composite films," *Journal of the Textile Institute*, vol. 100, no. 3, pp. 254–259, 2009.

[48] C. S. Allen, F. Ghamouss, O. Boujibar, and P. J. F. Harris, "Aberration-corrected transmission electron microscopy of a non-graphitizing carbon," *Proceedings of the Royal Society A: Mathematical, Physical and Engineering Sciences*, vol. 478, no. 2258, p. 20210580, 2022.

[49] A. G. Gómez-Rojas, L. A. Macclesh-del Pino-Pérez, C. F. Castro-Guerrero, C. E. Ramos-Galván, and A. B. Morales-Cepeda, "Electrochemical oxidation of Pb II using carbon electrodes doped with nanocellulose-FeOx," *Fibers*, vol. 11, no. 1, p. 8, 2023.

[50] M. M. Mian, I. M. L. Kamana, X. An et al., "Cellulose nanofibers as effective binders for activated biochar-derived high- performance supercapacitors," *Carbohydrate Polymers*, vol. 301, no. B, article 120353, 2023.

[51] Q. Chen, M. Kang, Z. Rong, and Z. Zong, "Effect of cellulose nanocrystals on the performance of oil-immersed transformer insulating paper," *BioResources*, vol. 14, no. 3, pp. 6837–6850, 2019.

[52] X. Sun, X. Zhang, H. Zhang, D. Zhang, and Y. Ma, "A comparative study of activated carbon-based symmetric supercapacitors in Li_2SO_4 and KOH aqueous electrolytes," *Journal of Solid State Electrochemistry*, vol. 16, no. 8, pp. 2597–2603, 2012.

[53] R. de Levie, "On porous electrodes in electrolyte solutions: I. capacitance effects," *Electrochimica Acta*, vol. 8, no. 10, pp. 751–780, 1963.

[54] H. Keiser, K. D. Beccu, and M. A. Gutjahr, "Abschatzung der porenstruktur poroser elektroden aus impedanzmessungen," *Electrochimica Acta*, vol. 21, no. 8, pp. 539–543, 1976.

[55] C. Xu, H. Du, B. Li, F. Kang, and Y. Zeng, "Asymmetric activated carbon-manganese dioxide capacitors in mild aqueous electrolytes containing alkaline-earth cations," *Journal of the Electrochemical Society*, vol. 156, no. 6, p. A435, 2009.

[56] S. Lee, B. Gendensuren, B. Kim et al., "Effect of emulsified polymer binders on the performance of activated carbon electrochemical double-layer capacitors," *Korean Journal of Chemical Engineering*, vol. 36, p. 1940, 2019.